Hindawi Publishing Corporation
Mathematical Problems in Engineering
Volume 2015, Article ID 525921, 8 pages
http://dx.doi.org/10.1155/2015/525921

Research Article

Probabilistic Risk Assessment: Piping Fragility due to Earthquake Fault Mechanisms

Bu Seog Ju,[1] WooYoung Jung,[2] and Myung-Hyun Noh[3]

[1] *Department of Civil Engineering, North Carolina State University, Raleigh, NC 27695, USA*
[2] *Department of Civil Engineering, Gangneung-WonJu National University, Gangneung 210-702, Republic of Korea*
[3] *Steel Solution Center, POSCO, 100 Songdo Gwahak-ro, Yeonsu-gu, Incheon 406-840, Republic of Korea*

Correspondence should be addressed to Myung-Hyun Noh; mnoh@posco.com

Received 28 July 2014; Accepted 15 September 2014

Academic Editor: Sang-Youl Lee

A lifeline system, serving as an energy-supply system, is an essential component of urban infrastructure. In a hospital, for example, the piping system supplies elements essential for hospital operations, such as water and fire-suppression foam. Such nonstructural components, especially piping systems and their subcomponents, must remain operational and functional during earthquake-induced fires. But the behavior of piping systems as subjected to seismic ground motions is very complex, owing particularly to the nonlinearity affected by the existence of many connections such as T-joints and elbows. The present study carried out a probabilistic risk assessment on a hospital fire-protection piping system's acceleration-sensitive 2-inch T-joint sprinkler components under seismic ground motions. Specifically, the system's seismic capacity, using an experimental-test-based nonlinear finite element (FE) model, was evaluated for the probability of failure under different earthquake-fault mechanisms including normal fault, reverse fault, strike-slip fault, and near-source ground motions. It was observed that the probabilistic failure of the T-joint of the fire-protection piping system varied significantly according to the fault mechanisms. The normal-fault mechanism led to a higher probability of system failure at locations 1 and 2. The strike-slip fault mechanism, contrastingly, affected the lowest fragility of the piping system at a higher PGA.

1. Introduction

In the event of earthquake, the fire-protection piping system (sprinkler piping system), as an essential nonstructural component in critical facilities such as hospitals, emergency clinics, and high-tech factories, must remain secure and operational in order to prevent the damage from fire. Interestingly, many previous reports have attributed the most serious earthquake damage to the poor performance of nonstructural components such as HVAC, ceiling system, and fire-protection piping system [1] rather than to structural components. The Olive View Hospital, for example, seismically retrofitted after the 1971 San Fernando earthquake, did not incur any structural damage from the 1994 Northridge event. However, due to leakages from the fire-protection piping system and the chilled water distribution system, the hospital had to be shut down, further necessitating the evacuation of 377 patients [2]. During the 1995 Kobe earthquake in Japan, 40.8% of fire-suppression systems such as sprinkler piping systems were damaged [3], due to the acute seismic vulnerability of sprinkler piping systems (as part of fire-protection piping systems) relative to other fire-suppression systems such as indoor fire hydrants, foam-based extinguishing systems, and fire doors.

In order to prevent or minimize damage from fire, hospitals' nonstructural components including automatic fire alarm systems, HVAC systems, and fire-protection piping systems (sprinkler piping systems) must remain operational and functional both during and after earthquakes. In recent years, significant research has been conducted to evaluate the seismic performance and vulnerability of fire-protection piping systems in hospitals according to earthquake engineering principles. Antaki and Guzy [4] performed a seismic performance analysis of a fire-protection piping system incorporating grooved and threaded connections. Also, the University of Buffalo [5, 6] conducted experimental tests on

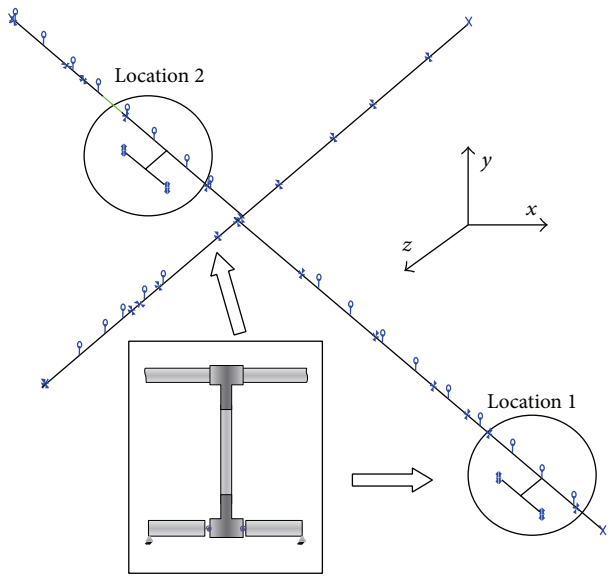

Figure 1: Sprinkler piping system configuration with multibranch systems [7].

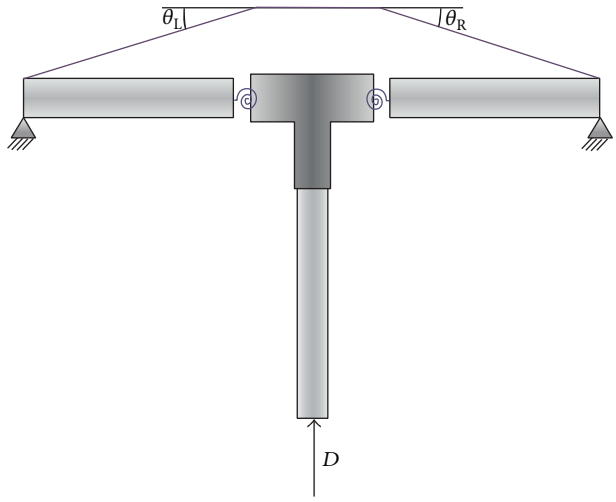

Figure 2: FE model of T-joint system [8].

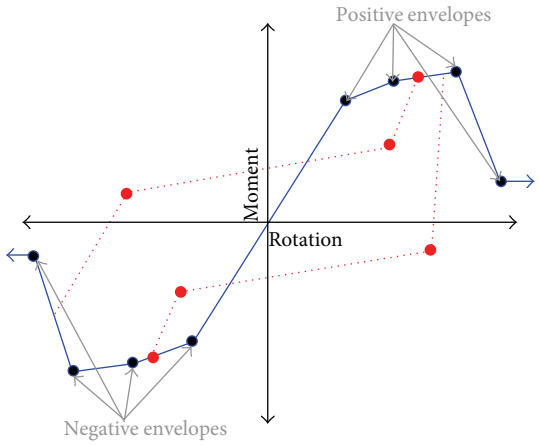

Figure 3: *Pinching4* material in *OpenSees* [9].

a sprinkler piping system under monotonic and cyclic loading conditions, with respect to two connection types (threaded T-joint and grooved T-joint) and two materials (black iron and chlorinated polyvinyl chloride (CPVC)).

Based on the outcomes of relevant previous investigations [7, 8, 11], the present study, in order to reduce seismic-induced fire risk and develop a probabilistic risk assessment protocol for sprinkler piping systems in hospitals, (1) incorporated an analytical and numerical nonlinear T-joint model specified by experimental-test-derived moment-rotation relationships, (2) considered various seismic ground-motion intensities and various fault mechanisms as a function of uncertainties, (3) conducted multiple nonlinear time-history analyses for a Monte Carlo simulation, and (4) estimated the system's change of probabilistic failure and acceleration sensitivity according to various earthquake-fault mechanisms.

2. Fire-Protection Piping System

Taking the lead of Ju and Jung [7], a hospital's top-floor main piping system (designed according to the NFPA-13 [12] and SMACNA [13] seismic guidelines), with two nonlinear T-joint branch systems supported by unbraced single hangers, transverse braced hangers, and longitudinal braced hangers, was selected for the purposes of the present study. The particular locations of the multibranch piping systems were determined, by linear time-history analysis of the complete piping system, to be the first and second maximum displacements and rotations. Figure 1 illustrates the piping system configuration considered in this study. The natural frequencies of the piping system in the fundamental and second modes were 1.82 (Hz) and 3.28 (Hz), respectively.

2.1. Finite Element (FE) Model of T-Joint System [7]. The existence of many connections and linkages in a sprinkler piping system causes complex nonlinear behavior. In the study of nonlinear behavior by FE analysis, dense mesh and special contact elements often are required; however, considering these factors in fragility estimation can be computationally inefficient. Therefore, in the present study, a nonlinear moment-rotation relationship obtained from University of Buffalo (UB) cyclic-experimental data [5, 6] was used to generate the nonlinear FE model of a threaded T-joint in a 2-inch black iron branch piping system. Figure 2 provides a schematic of the FE model, which represents the system's nonlinear behavior by two nonlinear rotational springs. Smaller rotations were allowed by means of a hinge supporting the branch pipes. The load was applied at the bottom along the perpendicular axis. The *Pinching4* uniaxial material was applied on the *OpenSees* platform [14]. The *Pinching4* material shown in Figure 3 used various parameters such as positive and negative response envelopes, the ratio of deformation, force, and strength under unloading conditions, and the ratio of deformation, force, and strength under reloading conditions. Furthermore, the *Pinching4* material model was able to represent the stiffness degradation, the strength

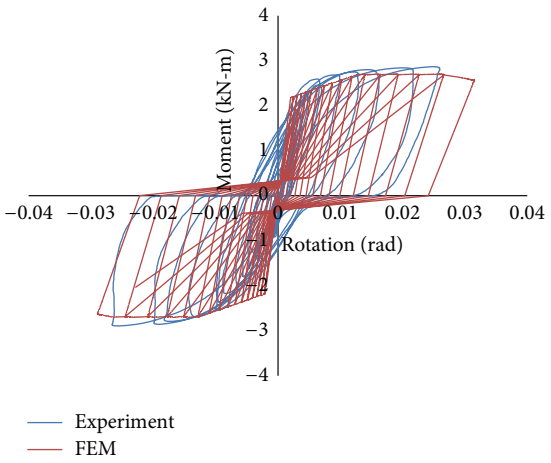

Figure 4: Validation of FE model for 2-inch threaded T-joint system [8].

degradation, and the unloading/reloading conditions under cyclic loading [9]. Figure 4 plots the validation data on the FE model for the threaded T-joint system. The moment-rotation relationship obtained in the FE analysis was in good agreement with the experimental values.

3. Seismic Ground Motions

Damage to a nonstructural fire-protection piping system subjected to seismic ground motions is a function of the strength and deformation capacity of each component. Damage to structural and nonstructural components, meanwhile, correlates with both input and dissipated energy [15]. In the present study, various ground motions, namely, normal-fault, reverse-fault, strike-slip fault, and near-source ground motions, were applied in order to investigate the effect of input and dissipated energy on the piping system. Ground motions over the Richter magnitude M_w 6.0 were selected from PEER-NGA [16], and near-source ground motions influenced by a few pulses were borrowed from Sasani et al. [15]. Each earthquake dataset was normalized to the same peak ground acceleration (PGA) (1.0 g). Figures 5(a) to 5(d) provide the response spectra for a 5% damping ratio. The thick solid curve indicates the mean value of the response spectra.

The dynamic equation of motion for this piping system subjected to earthquakes can be expressed as

$$[M]\{\ddot{u}(t)\} + [C]\{\dot{u}(t)\} + [K]\{u(t)\} = -[M]\left\{\ddot{u}_g(t)\right\}, \quad (1)$$

where M, C, K, and $\ddot{u}_g(t)$ are mass, damping, stiffness, and ground acceleration, respectively. In particular, Rayleigh classical damping known as mass and stiffness proportional damping was used in order to generate damping matrix. The damping equation is as follows:

$$[C] = \alpha[M] + \beta[K]. \quad (2)$$

The mass and stiffness coefficients (α and β) can be described as follows:

$$\frac{1}{2}\begin{bmatrix} \frac{1}{\omega_i} & \omega_i \\ \frac{1}{\omega_j} & \omega_j \end{bmatrix}\begin{Bmatrix}\alpha\\ \beta\end{Bmatrix} = \begin{Bmatrix}\xi_i\\ \xi_j\end{Bmatrix}, \quad (3)$$

in which ω_i and ω_j are the natural frequency for the ith and jth modes. Also, ξ_i and ξ_j are the specified damping ratios for the ith and jth modes [17]. Specifically, in this study, 2% damping ratio was applied for the black iron piping system.

4. Probabilistic Risk Assessment of Piping System

Probabilistic risk assessment and performance-based design are practical approaches to the mitigation of potential fire, hurricane, or earthquake damage to structural systems [18]. Additionally, the Electric Power Research Institute (EPRI) recently formulated a fragility analysis methodology for use in probabilistic risk assessment (PRA) of nuclear power plants [19]. According to Shinozuka et al. [20], the empirical fragilities based on lognormal distribution function were classified into two different methods: (1) Parameter Estimation (Method 1) by means of the maximum likelihood procedure and (2) Parameter Estimation (Method 2) by log-standard deviation along with the medians of the lognormal distribution in terms of the aid of maximum likelihood method. The maximum likelihood function for Method 1 can be expressed as

$$L = \prod_{i=1}^{N}[F(a_i)]^{x_i}[1 - F(a_i)]^{1-x_i}, \quad (4)$$

where $F(a_i)$ indicates the probability of failure with respect to the specified damage level and the analytical solution for the fragility curve was given by

$$F(\cdot) = \Phi\left[\frac{\ln(a/c)}{\varsigma}\right], \quad (5)$$

where parameter "a" is peak ground acceleration (PGA).

Furthermore, the fragility (Method 2) corresponding to four damage states (E_1, E_2, E_3, and E_4) is described by two parameters: median (m_c) and lognormal standard deviation (β_{sd}) given in

$$F(\cdot) = \Phi\left[\frac{\ln(a_i/m_c)}{\beta_{\mathrm{sd}}}\right]. \quad (6)$$

The probability of failure for each damage state (no damage, minor, moderate, and major damage) at given PGA levels was also described as follows:

$$\begin{aligned} P_1 &= P(a_i, E_1) = 1 - F_1(\cdot), \\ P_2 &= P(a_i, E_2) = F_1(\cdot) - F_2(\cdot), \\ P_3 &= P(a_i, E_3) = F_2(\cdot) - F_3(\cdot), \\ P_4 &= P(a_i, E_4) = F_3(\cdot). \end{aligned} \quad (7)$$

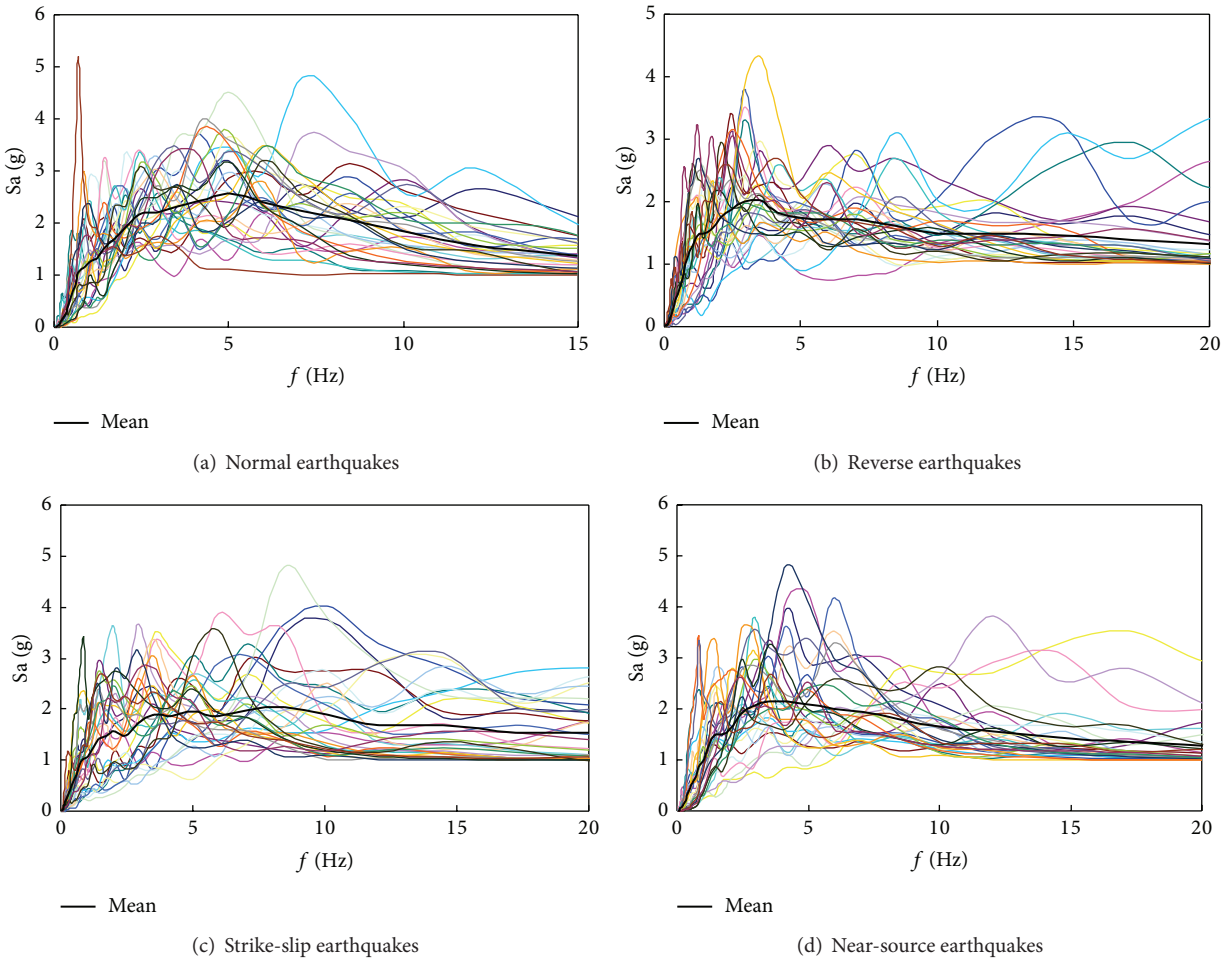

FIGURE 5: Seismic ground motions: response spectra based on fault mechanisms.

In this case, the likelihood function can be generalized as

$$L(\cdot) = \prod_{i=1}^{N}\prod_{j=1}^{4} P_j\left(a_i; E_j\right)^{x_{ij}}. \tag{8}$$

Further details for the analytical fragility methodology can be found in the study by Shinozuka et al. [20].

Based on this fragility analysis (Parameter Estimation: Method 2), Ju et al. [8] defined the probability of failure of a fire-protection piping system as follows:

$$\begin{aligned} P_f(\lambda) &= P\left[G(\cdot) < 0 \mid \text{Earthquake Intensity} = \lambda\right], \\ P_f(\lambda) &= P\left[C < D \mid \text{PGA} = \lambda\right], \end{aligned} \tag{9}$$

in which $G(\cdot)$ represents failure limit state, C is the capacity or strength of the system, and D is the load or demand.

Nonstructural fragilities, which are engineering demand parameter (EDP) functions, indicate the probabilities that certain nonstructural components will exceed a certain level of damage [18]. Equation (9) above formulates fragility for a peak ground acceleration (PGA) level of λ.

Structural fragilities, meanwhile, are estimated empirically by conducting multiple nonlinear time-history analyses of a structure for various ground motions:

$$P_f(\lambda) = \frac{\sum_{i=1}^{N} 1\left(\theta_{i,\lambda} \geq \theta_{\text{lim}} \mid \text{PGA} = \lambda\right)}{N}. \tag{10}$$

In (10), $\theta_{i,\lambda}$ is the maximum rotation from the ith earthquake time-history analysis at a PGA level of λ, and $1(\cdot)$ is the indicator function.

5. Limit State of 2-Inch T-Joint System

As (9) and (10) reflect, it was necessary to characterize the limit state criteria corresponding to fire-protection piping system damage. Failure due to leakage generally predominated over support system failure in this study. Therefore, the American Society of Mechanical Engineers (ASME) BPVP code (Section 3) defined rotation corresponding to plastic collapse of piping components using the "twice the elastic slope" (TES) criteria [8]. Based on these criteria, the rotation corresponding to plastic collapse θ_φ can be determined by the abscissa of the point at which a line with twice the elastic

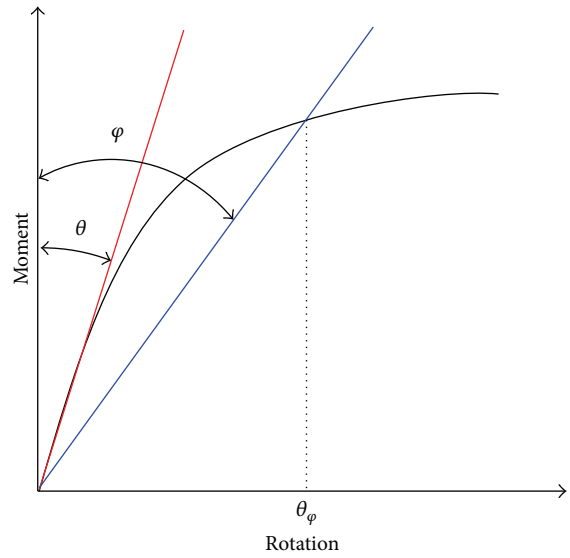

Figure 6: Twice elastic slope (TES) criteria [8].

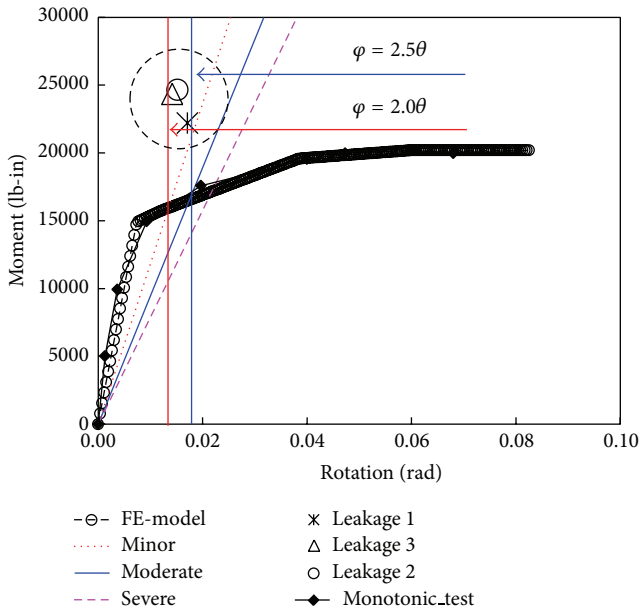

Figure 7: Damage states of 2-inch threaded T-joint piping system [8].

slope intersects the moment-rotation curve. This condition is exemplified in Figure 6, where $\varphi = 2\theta$. In Figure 7, the rotations of the left spring corresponding to the "First-Leak" damage state during three cyclic tests are plotted along with the moment-rotation relationship obtained from the experimental data. It can be seen that all three failure rotations lay between the lines $\varphi = 2\theta$ and $\varphi = 2.5\theta$, where θ is the elastic slope. It can be concluded that the TES ($\varphi = 2\theta$) criteria can be conservatively assumed as the limit state corresponding to the "First Leak" (0.0135 radians) [8]. Hence, three damage states are defined by minor (0.0135 rad), moderate (0.0175 rad), and severe damage (0.0217 rad), respectively.

6. Seismic Fragility of Fire-Protection Piping Systems Subjected to Various Fault Mechanisms

The piping-system seismic fragility evaluation presented in this paper was based on analyses of multiple nonlinear time-histories as functions of uncertainties such as magnitude, soil types, and fault mechanisms. The evaluation proceeds as follows.

(1) Select seismic ground motions of each fault mechanism (normal, reverse, and strike-slip) and near-source ground motions as functions of uncertainties.

(2) Incorporate the nonlinear T-joint FE model into the main piping system based on the experimental result.

(3) Perform multiple nonlinear time-history analyses by means of a Monte Carlo simulation (MCS) of the fire-protection piping system on the *OpenSees* platform.

Finally, from the numerical analyses, the absolute maximum inelastic rotations were obtained, and the numerical fragility curves for the three different fault mechanisms and near-source ground motions were evaluated by (10). Figure 8 showed the procedure of system fragility analysis based on Monte Carlo simulation [10]. The nonlinear time-history analyses were conducted at many PGA levels ranging from 0.2 g to 4.0 g increments.

The fragility estimates (i.e., probabilities of failure) corresponding to the piping system's limit state of inelastic rotation (0.0135 radians) for each fault mechanism case are compared in Figure 9. The fragility of a fire-protection piping system subjected to 50 seismic ground motions (50 EQs) was determined by Ju and Jung [7]. As shown in the figure, the probability of failure at location 1 significantly differed among the four earthquake types. The piping system subjected to 50 EQs was most fragile under the normal-fault mechanism and yielded greatly. The fragility values according to the reverse and near-source ground motions tended to show similar probabilities of failure. The maximum probability difference, between the normal- and strike-slip fault mechanisms, was approximately 40% at the PGA of 1.8 g.

Figure 10 plots the probabilities of failure at location 2. Overall, the fragility values there were lower than at location 1. The fragility as subjected to the normal-fault mechanism was highly conservative, showing a similar pattern to that indicated in Figure 9. However, the values with respect to the probability of failure at location 2 under the reverse-fault mechanism were significantly lower than the other values up to the PGA of 2.5 g. The maximum fragility difference, this time between the normal- and reverse-fault mechanisms, was approximately 41% at the PGA of 2.2 g. Also, analytical fragility curves (solid lines) for each case are evaluated by (6) and median and lognormal standard deviation (Table 1) is obtained from numerical fragility analyses (MCS). Based on (7), Figure 11 illustrates the damage-state (minor, moderate, and severe damage) probabilities of the piping system subjected to normal earthquake-fault mechanism at locations 1 and 2.

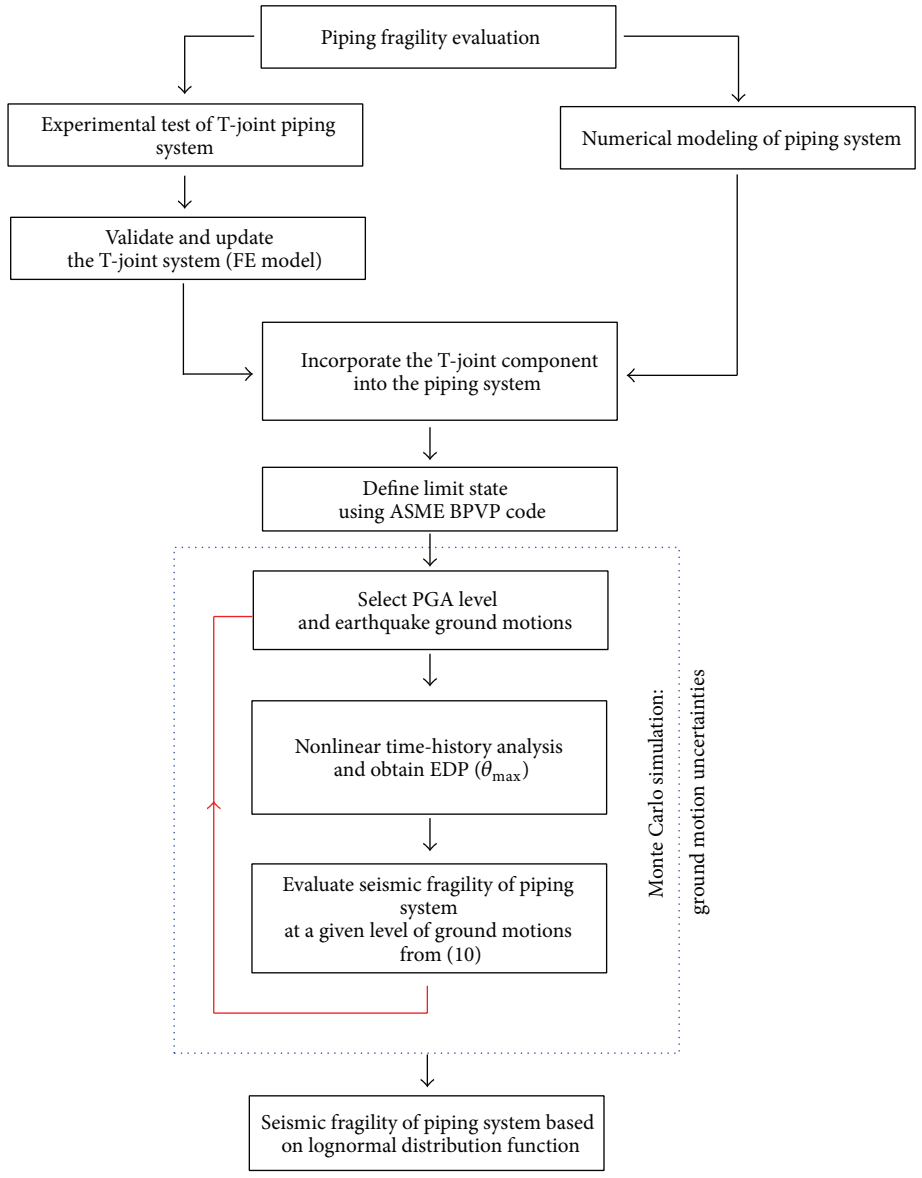

Figure 8: Flowchart of seismic fragility of piping system [10].

Table 1: Median and lognormal standard deviation variables.

Fault mechanisms	Location 1		Location 2	
	m_c	β_{sd}	m_c	β_{sd}
Normal	0.4835	0.2534	0.6264	0.3594
Reverse	0.6679	0.3945	0.9095	0.2598
Strike-slip	0.8144	0.5210	0.9270	0.5167
Near-source	0.6752	0.2948	0.7792	0.3963
50 EQs	0.4144	0.3741	0.6771	0.3398

In addition, in order to generate entire fragility corresponding to particular damage state, the ground acceleration capacity (A) related to median ground acceleration capacity (a_m) and lognormal random variables ($\varepsilon_R\varepsilon_U$) in terms of the median and uncertainty in the median value must be defined by [21]

$$A = a_m\varepsilon_R\varepsilon_U. \tag{11}$$

Therefore, the median PGA capacities (50% probability of failure) at locations 1 and 2 are listed in Table 2. The primary reason for the differences among the fragility values was the sensitive response of the piping system to the seismic ground-motion frequency and acceleration.

7. Conclusions

This study developed a framework for probabilistic risk assessment of fire-protection piping systems (sprinkler piping systems) subjected to various earthquake-fault mechanisms in order to improve their seismic performance and reduce

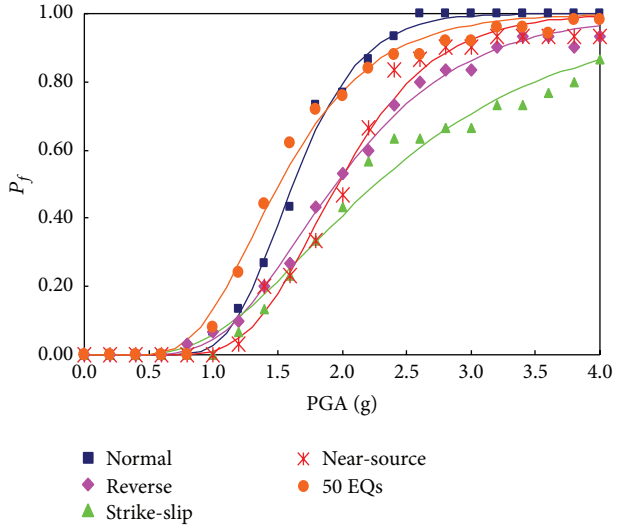

Figure 9: Probabilities of failure of fire-protection piping system at location 1.

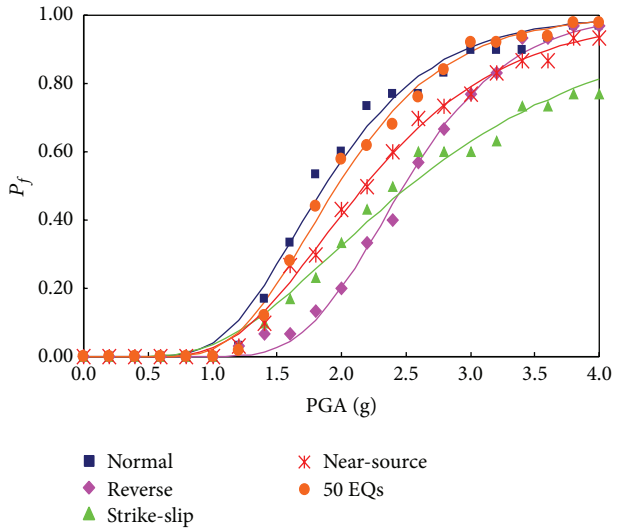

Figure 10: Probabilities of failure of fire-protection piping system at location 2.

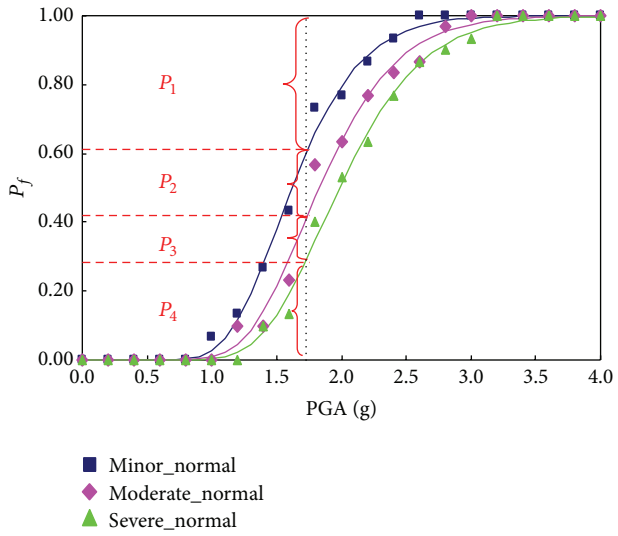

(a) Damage states' probabilities at location 1

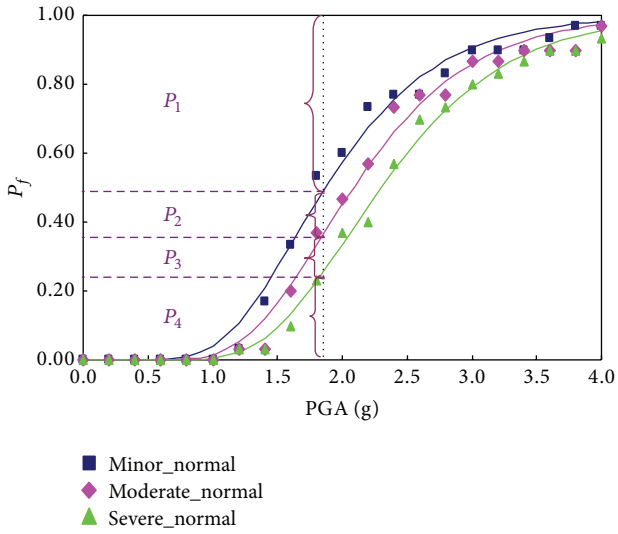

(b) Damage states' probabilities at location 2

Figure 11: Probabilities of failure corresponding to the damage states.

Table 2: Median PGA capacities.

Fault mechanisms	Location 1 (g)	Location 2 (g)
Normal	1.624	1.872
Reverse	1.960	2.484
Strike-slip	2.260	2.548
Near-source	1.968	2.184
50 EQs	1.524	1.972

seismic-induced fire damage during and after an earthquake. A stochastic seismic analysis was performed on a 2-inch black iron multibranch piping system represented by a nonlinear FE model. A Monte Carlo simulation was conducted in order to evaluate the system-level fragility of T-joint piping system. Based on the finding from simulation, the fragility curves properly fitted into a lognormal cumulative distribution. The overall study results showed that the failure probabilities at locations 1 and 2 differ significantly by fault mechanism. The fragility according to the normal-fault mechanism was similar to the fragility of the piping system as subjected to 50 EQs at locations 1 and 2. This normal-fault fragility was extremely conservative or, in other words, exceedingly fragile. The maximum difference between the different fault types was approximately 40% at both locations 1 and 2. This suggests that seismic ground-motion acceleration and frequency in piping systems that include acceleration-sensitive components can have a considerable effect on fragility. Indeed, this was the rationale for the present study's evaluation of the seismic capacities of the T-joint sprinkler piping components. Further evaluation of the interaction between buildings and their fire-protection piping systems and of the dynamic

impact influence between ceiling systems and sprinkler heads remains for future work.

Conflict of Interests

The authors declare that there is no conflict of interests regarding the publication of this paper.

Acknowledgment

This research was supported by a Grant (13SCIPA01) from Smart Civil Infrastructure Research Program funded by the Ministry of Land, Infrastructure and Transport (MOLIT) of Korea Government and Korea Agency for Infrastructure Technology Advancement (KAIA) and supported by a National Research Foundation of Korea (NRF) grant funded by the Korean government (MEST) (no. 2012-0008762).

References

[1] N. C. Gould and M. J. Griffin, "The value of seismically installing and strengthening non-structural equipment and systems to significantly reduce business interruption losses," in *Proceedings of the Seminar on Seismic Design, Performance, and Retrofit of Nonstructural Components in Critical Facilities*, ATC-29-2, Newport Beach, Calif, USA, 2003.

[2] M. Shinozuka and S. Masri, "Seismic risk assessment of nonstructural components in hospitals," in *Proceedings of Seminar on Seismic Design, Performance, and Retrofit of Nonstructural Components in Critical Facilities*, Newport Beach, Calif, USA, 2003.

[3] A. I. Sekizawa, M. Ebihara, and H. Notake, "Development of seismic-induced fire risk assessment method for a building," in *Proceedings of the 7th International Symposium on Fire Safety Science*, pp. 309–320, June 2003.

[4] G. Antaki and D. Guzy, "Seismic testing of grooved and threaded fire protection joints and correlation with nfpa seismic design provisions," in *Proceedings of the ASME Pressure Vessels & Piping Conference*, vol. 364, pp. 69–75, 1998.

[5] J. Dow, "Testing and analysis of iron and plastic T-joint in sprinkler systems," NEESR–GC: "Simulation of the Seismic Performance of Nonstructural Systems", 2010, https://nees.org/site/resources/pdfs/REU2009_Dow_Paper.pdf.

[6] Y. Tian, J. Fuchs, G. Mosqueda, and A. Filiatrault, "NEESR Nonstructural: progress report on tests of Tee Joint component of sprinkler piping system," Progress Report, NEESR-GC: Simulation of the Seismic Performance of Nonstructural Systems, 2010.

[7] B. S. Ju and W. Y. Jung, "Seismic fragility evaluation of multibranch piping systems installed in critical low-rise buildings," *Disaster Advances*, vol. 6, no. 4, pp. 59–65, 2013.

[8] B. S. Ju, S. K. Tadinada, and A. Gupta, "Fragility analysis of threaded T-joint connections in hospital piping systems," in *Proceedings of the ASME Pressure Vessels and Piping Conference (PVP '11)*, vol. 8, pp. 147–155, Baltimore, Md, USA, July 2011.

[9] S. Mazzoni, F. McKenna, M. H. Scoot, and G. L. Fenves, *OpenSees Command Language Manual*, 2006, http://opensees.berkeley.edu/.

[10] B. S. Ju and W. Y. Jung, "Framework for fragility evaluation of piping system," in *Proceedings of the 22nd Conference on Structural Mechanics in Reactor Technology (SMiRT '22)*, San Francisco, Calif, USA, August 2013.

[11] B. S. Ju, W. Y. Jung, and Y. H. Ryu, "Seismic fragility evaluation of piping system installed in critical structures," *Structural Engineering and Mechanics*, vol. 46, no. 3, pp. 337–352, 2013.

[12] NFPA-13, *Standard for the Installation of Sprinkler System*, National Fire Protection Association, Quincy, Mass, USA, 2007.

[13] SMACNA, *Seismic Restraint Manual Guidelines for Mechanical Systems*, Sheet Metal and Air Conditioning Contractors' National Association, Inc., 2003.

[14] OpenSees, *Open System for Earthquake Engineering Simulation*, http://opensees.berkeley.edu/.

[15] M. Sasani, A. der Kiureghian, and V. V. Bertero, "Seismic fragility of short period reinforced concrete structural walls under near-source ground motions," *Structural Safety*, vol. 24, no. 2-4, pp. 123–138, 2002.

[16] PEER-NRG, Pacific Earthquake Engineering Research Center: NGA Database, http://peer.berkeley.edu/nga/.

[17] A. K. Chopra, *Dynamics of Structures*, Prentice Hall, New York, NY, USA, 2nd edition, 2007.

[18] K. Porter and R. Bachman, "Developing fragility functions for building components for ATC-58," ATC-58 Nonstructural Products Team, 2006, http://www.sparisk.com/pubs/Porter-2006-deriving-fragility.pdf.

[19] Electric Power Research Institute (EPRI), "Methodology for developing seismic fragilities," TR-103959 Research Project, Electric Power Research Institute (EPRI), 1994.

[20] M. Shinozuka, M. Q. Feng, H. Kim, T. Uzawa, and T. Ueda, "Statistical analysis of fragility curves," Technical Report MCEER, FHWA Contract Number: DTFH61-92-C-00106, 2001.

[21] M. K. Ravindra, *Probabilistic Structural Mechanics Handbook: Seismic Risk Assessment*, Chapman & Hall, Springer, New York, NY, USA, 1995.